

## Article

# Unraveling the Effect of MgAl/CuO Nanothermite on the Characteristics and Thermo-Catalytic Decomposition of Nanoenergetic Formulation Based on Nanostructured Nitrocellulose and Hydrazinium Nitro-Triazolone

Mohammed Dourari <sup>1</sup>, Ahmed Fouzi Tarchoun <sup>2,\*</sup> , Djalal Trache <sup>1,\*</sup> , Amir Abdelaziz <sup>1</sup>, Slimane Bekhouche <sup>1</sup>, Abdelatif Harrat <sup>1</sup>, Hani Boukeciat <sup>1</sup> and Nawel Matmat <sup>1</sup>

<sup>1</sup> Energetic Materials Laboratory (EMLab), Teaching and Research Unit of Energetic Processes, Ecole Militaire Polytechnique, BP 17, Bordj El-Bahri 16046, Algeria

<sup>2</sup> Energetic Propulsion Laboratory, Teaching and Research Unit of Energetic Processes, Ecole Militaire Polytechnique, BP 17, Bordj El-Bahri 16046, Algeria

\* Correspondence: tarchounfouzi@gmail.com (A.F.T.); djalaltrache@gmail.com (D.T.)

**Abstract:** The present study aims to develop new energetic composites containing nanostructured nitrocellulose (NNC) or nitrated cellulose (NC), hydrazinium nitro triazolone (HNTO), and MgAl-CuO nanothermite. The prepared energetic formulations (NC/HNTO/MgAl-CuO and NNC/HNTO/MgAl-CuO) were analyzed using various analytical techniques, such as Fourier-transform infrared (FTIR), scanning electron microscopy (SEM), thermogravimetry (TGA), and differential scanning calorimetry (DSC). The outstanding catalytic impact of MgAl-CuO on the thermal behavior of the developed energetic composites was elucidated by kinetic modeling, applied to the DSC data using isoconversional kinetic methods, for which a considerable drop in the activation energy was acquired for the prepared formulations, highlighting the catalytic influence of the introduced MgAl-CuO nanothermite. Overall, the obtained findings demonstrated that the newly elaborated NC/HNTO/MgAl-CuO and NNC/HNTO/MgAl-CuO composites could serve as promising candidates for application in the next generation of composite explosives and high-performance propellants.

**Keywords:** nitrocellulose; nanostructured nitrocellulose; hydrazinium nitro triazolone; nanocatalyst; energetic composite; thermo-kinetics



**Citation:** Dourari, M.; Tarchoun, A.F.; Trache, D.; Abdelaziz, A.; Bekhouche, S.; Harrat, A.; Boukeciat, H.; Matmat, N. Unraveling the Effect of MgAl/CuO Nanothermite on the Characteristics and Thermo-Catalytic Decomposition of Nanoenergetic Formulation Based on Nanostructured Nitrocellulose and Hydrazinium Nitro-Triazolone. *Catalysts* **2022**, *12*, 1573. <https://doi.org/10.3390/catal12121573>

Academic Editors: Dezhi Han, Wentai Wang and Ning Han

Received: 2 November 2022

Accepted: 30 November 2022

Published: 3 December 2022

**Publisher's Note:** MDPI stays neutral with regard to jurisdictional claims in published maps and institutional affiliations.



**Copyright:** © 2022 by the authors. Licensee MDPI, Basel, Switzerland. This article is an open access article distributed under the terms and conditions of the Creative Commons Attribution (CC BY) license (<https://creativecommons.org/licenses/by/4.0/>).

## 1. Introduction

The term “energetic materials” (EMs) refers to a class of chemical compounds that, when stimulated using various possible methods (e.g., external mechanical, thermal forces, laser ignition), rapidly release a significant amount of stored chemical energy. They consist of pyrotechnics, explosives, and propellants, with several uses in ordnance, rockets, missiles, gas generators, space technology, car airbags, demolition, welding, and mining [1,2]. The most widely used energetic ingredient, since the 19th century, is nitrocellulose (NC), in both the defense and non-defense sectors, owing to its inherent characteristics, which include easy tunability, high flammability, explosiveness, and excellent mechanical features [3–5]. The intrinsic properties of conventional NC can be further enhanced by structurally altering its cellulosic precursor to design nanostructured nitrocellulose (NNC), which has the potential to be used in formulations with high levels of energy density [6]. This innovative class of nitrated cellulose derivatives displayed enhanced physicochemical properties and energetic performance with regard to the traditional NC, making it a highly desirable substitute candidate for the development of new, high-value cellulosic products for prospective use in advanced energetic formulations [7,8]. Another frequently used component in NC-based propellants is nitroglycerine (NG), while its replacement has been commonly demanded because of its migration problems and decreased stability [9,10]. In

order to move past these limitations and reduce the reliance on nitroglycerine, various types of emergent energetic additives, such as nitramine explosives [11,12], green oxidizers [13], energy-rich ionic liquids [14], energetic co-crystals [15], and nanothermites [16], have already been introduced in NC-based composites to assess their effectiveness and find the next generation of energetic formulations. Currently, considerable attention has been concentrated on nitrogen-rich heterocyclics due to their attractive features, such as improved thermal stability, reduced sensitivities, and good compatibility with other compounds [17,18]. One of them, hydrazinium nitro-triazolone (HNTO), is an energetic salt that has been successfully developed by the reaction of 3-nitro-1,2,4-triazol-5-one (NTO) with hydrazine hydrate [19], and it has extremely appealing qualities that encourage its use in composite explosives and solid propellants [20,21]. Other additives that have attracted attention are metastable intermixed composites (MICs), also called nanothermites [22]. These additives are mainly composed of metal and metalloid fuel nanoparticles (e.g., Al, Si, Mg) and an oxidizer (e.g., CuO, Fe<sub>2</sub>O<sub>3</sub>, NiO), which rapidly generate exothermic energy when the ignition is initiated. This class of energetics has a far higher energy density than explosives [23–25]. Thermite reactions involving CuO and Al may reach temperatures of 2840 K, and their volumetric energy density is around three-times higher than that of trinitrotoluene (TNT) [26]. MICs offer exceptional catalytic effects on the components of solid propellants, owing to their high specific surface area and active sites [27,28].

In this study, composite films based on NC (or NNC)/HNTO/MgAl-CuO were designed and fully analyzed using various analytical tools, including Fourier-transform infrared (FTIR), scanning electron microscopy (SEM), thermogravimetry (TG) and differential scanning calorimetry (DSC). The kinetic triplet, namely, activation energy ( $E_a$ ), pre-exponential factor ( $\text{Log}(A)$ ), and reaction model ( $g(\alpha)$ ) of the developed NC (or NNC)/HNTO/MgAl-CuO composites, was calculated using isoconversional kinetic approaches. The acquired findings were also contrasted with those of other nano-energetic formulations that have been previously published.

## 2. Results

### 2.1. Chemical Structure and Morphology

The chemical functionalities of the elaborated NC (or NNC)/HNTO/MgAl-CuO composites were identified by Fourier-transform infrared spectroscopy (FTIR) and the recorded spectra are illustrated in Figure 1, also containing the spectra of raw NC (or NNC) and HNTO for comparison. Based on the obtained spectra, it is clear that the formed energetic formulations include the main functional peaks of NC at 1650, 1270, 1080, and 830 cm<sup>-1</sup>, which are assigned to the asymmetric NO<sub>2</sub> stretching, CH<sub>2</sub> bending, stretching vibration of C-O group, and O-NO<sub>2</sub> stretching vibration, respectively [8,29]. It can be also revealed from the expanded composites' spectra that the typical functional groups of HNTO are located at 3350 cm<sup>-1</sup> and 3283 cm<sup>-1</sup> for N-H of hydrazine, 2735 cm<sup>-1</sup> for N-H of triazole ring, 1696 cm<sup>-1</sup> for C=O stretching, and 1319 cm<sup>-1</sup> and 1509 cm<sup>-1</sup> for symmetric stretching and asymmetric stretching C-NO<sub>2</sub>, respectively [19,20]. These results make it evident that the structures of raw NC (or NNC) and HNTO are not altered after the preparation process.

On the other hand, scanning electron microscopy (SEM) was executed to elucidate the morphological features of the developed energetic mixtures and the obtained micrographs are shown in Figure 2, including the SEM images of NC, NNC, and HNTO for comparison. It is clearly observed from Figure 2 that HNTO is shaped like a rectangle rod [30], NC has lengthy and separate fibrous strands with a rough surface [31], while NNC shows short fibers with a rough microstructure and rod-shaped fibrillar aggregates, also known as microcrystals, with an approximate diameter of 10 μm [8,29]. It can also be revealed from the reported SEM images that the prepared energetic NC/HNTO/MgAl-CuO and NNC/HNTO/MgAl-CuO composites exhibit a different morphology. The NC/HNTO/MgAl-CuO formulation presents a homogeneous structure with a uniform interspersions of MgAl-CuO nanothermite throughout the NC/HNTO matrix, which indi-

cates increased intermolecular interactions between the ingredients [32,33]. Meanwhile, the NNC/HNTO/MgAl-CuO formulation shows a rod-like crystallite network with excellent distribution of MgAl-CuO particles, indicating that the substitution of pristine NC with its nanostructured derivative is a more uniform dispersion of HNTO and MgAl-CuO particles. This efficient dispersion is mostly resulting from the enhanced interfacial contact between the different substances, which is expected to accelerate the thermolysis of the developed energetic formulations, as will be demonstrated later in the following sections.

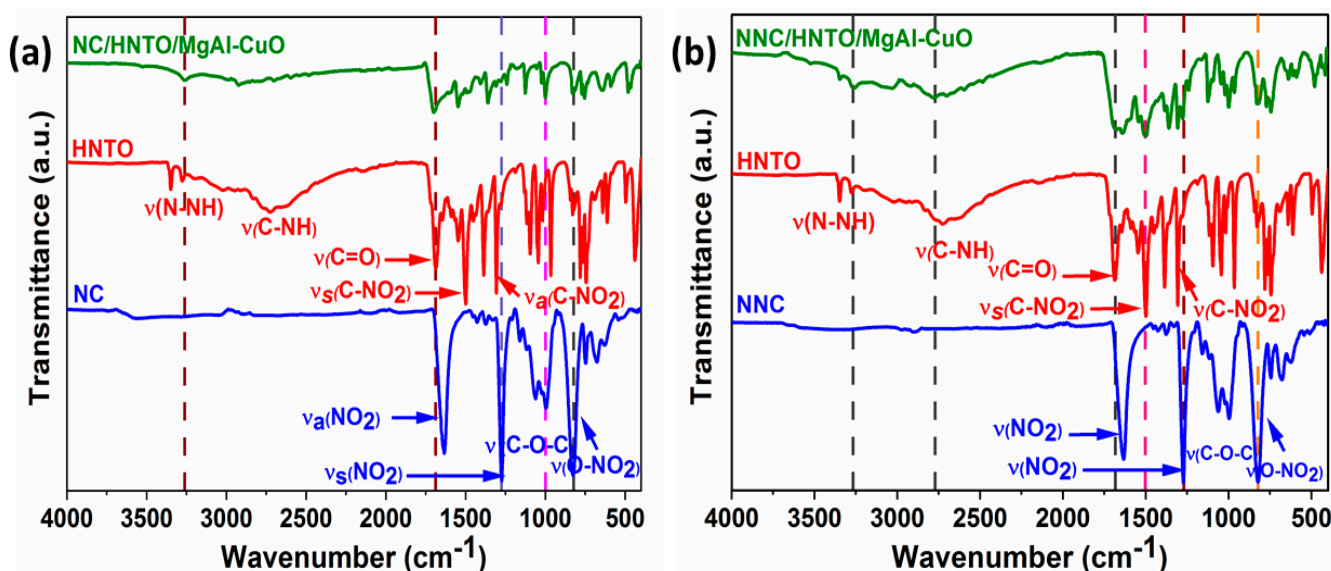


Figure 1. FTIR spectra of (a) NC/HNTO/MgAl-CuO composite; (b) NNC/HNTO/MgAl-CuO composite.

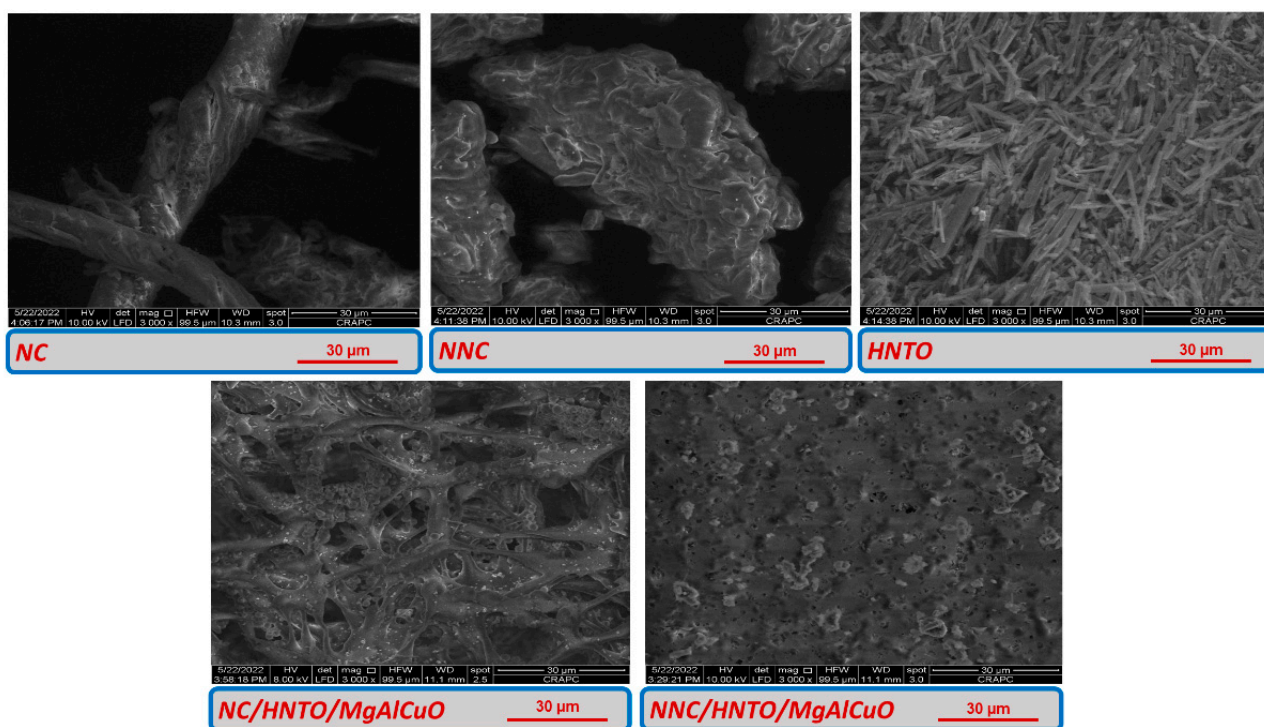
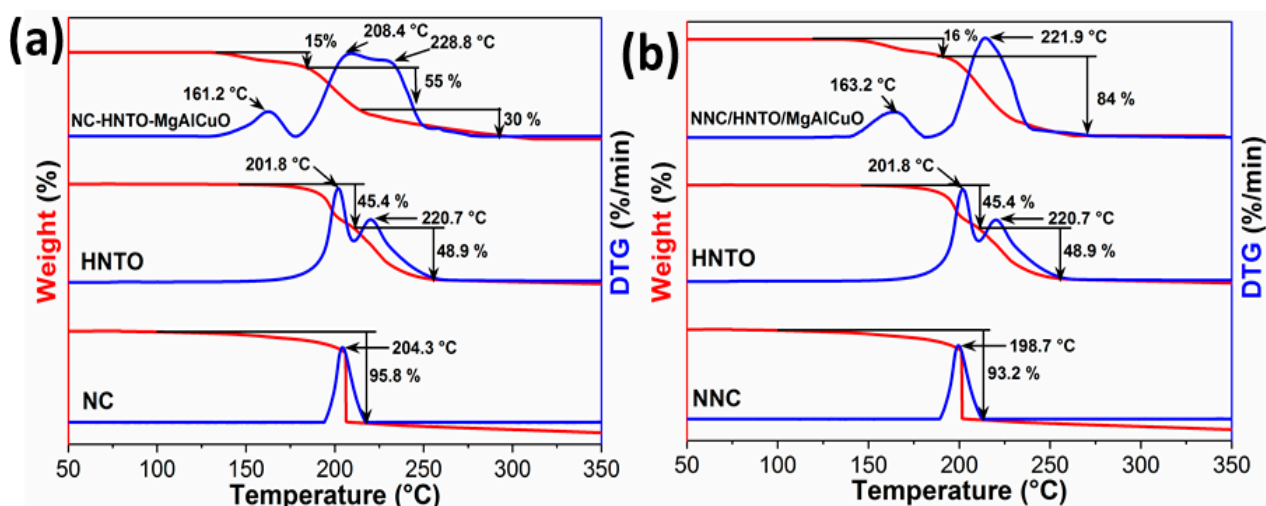


Figure 2. SEM images of the studied energetic composites and their raw constituents.

## 2.2. TGA Assessment

The thermal stability and decomposition behavior of the prepared energetic formulations were examined using the TGA, and their DTG thermograms are plotted in Figure 3, in

which both NC and NNC undergo a single mass-loss event ( $\sim 95\%$ ) at  $190\text{--}220\text{ }^{\circ}\text{C}$ . However, HNTO exhibits two successive decomposition stages at maximum peak temperatures of  $201\text{ }^{\circ}\text{C}$  and  $220\text{ }^{\circ}\text{C}$  with  $45.4\%$  and  $48.9\%$  weight losses, respectively. Regarding their chemical admixtures with MgAl-CuO nanothermite, NC/HNTO/MgAl-CuO displays a three-step decomposition that appeared at  $163\text{ }^{\circ}\text{C}$ ,  $208\text{ }^{\circ}\text{C}$ , and  $228\text{ }^{\circ}\text{C}$  with corresponding mass losses of around  $15\%$ ,  $55\%$ , and  $30\%$ , respectively. However, the NNC/HNTO/MgAl-CuO composite displays only two weightloss events of about  $16\%$  and  $84\%$ , recorded at  $161\text{ }^{\circ}\text{C}$  and  $221\text{ }^{\circ}\text{C}$ , respectively. According to these findings, we can conclude that the thermolysis behaviors of the obtained energetic formulations can be divided into the following parts: (1) the first decomposition linked to the thermolysis process of nitrated cellulosic chains through the homolytic splitting of O-NO<sub>2</sub> groups accompanied by the release of reactive radicals [34]; (2) the second part assigned to the decomposition stages of HNTO [35], wherein two events appeared in the case of the energetic composite based on NC and only one decomposition peak was found for the NNC-based energetic composite. This behavior can be explained by the catalytic impact of the MgAl-CuO combined with the good interfacial contact between NNC and HNTO, as confirmed by SEM analysis, which can offer additional oxidizing species that contribute to the entire oxidation of the existing fuel species [36,37]. Another outstanding feature is the shift in the exothermic processes of HNTO towards a higher temperature, specifying that the heat transfer from the reaction zone to the unburned parts of HNTO is sustained by nitrate esters, which promote the propagation of the exothermic process [38,39]. In addition, it can be revealed from Figure 3 that the energetic formulation based on NNC has lower thermal decomposition temperatures than that based on traditional nitrocellulose. This is due to the increased nitrogen content and reduced particle size of NNC, promoting the thermal reactivity of the resulting composite. This claim was supported by the findings reported by Dobrynin et al., who studied the feasibility of using supercritical antisolvent (SAS) processing to create nanoscale nitrocellulose (NC) [40]. They mentioned that nano-NC presents reduced friction sensitivity and lower decomposition temperatures than raw NC, while the early decomposition of NC/HNTO/MgAl-CuO and NNC/HNTO/MgAl-CuO composites compared to their NC and NNC matrices demonstrates the effective thermocatalytic effect of the used MgAl-CuO nanothermite [41].



**Figure 3.** TGA/DTG thermograms of the (a) NC/HNTO/MgAl-CuO and (b) NNC/HNTO/MgAl-CuO composites and their raw compounds at  $\beta = 10\text{ }^{\circ}\text{C}/\text{min}$ .

### 2.3. DSC Characterization

DSC studies have also been conducted at different heating rates (i.e.,  $10$ ,  $15$ ,  $20$ , and  $25\text{ }^{\circ}\text{C}/\text{min}$ ) to better understand the influence of MgAl-CuO nanothermite on the reactivity and energy output of the prepared energetic composites. Figure 4 shows the acquired

DSC curves of both energetic formulations at four heating rates, while Table 1 lists the heat released ( $\Delta H$ ), the measured onset and maximum decomposition temperatures ( $T_{onset}$  and  $T_{peak}$ ).

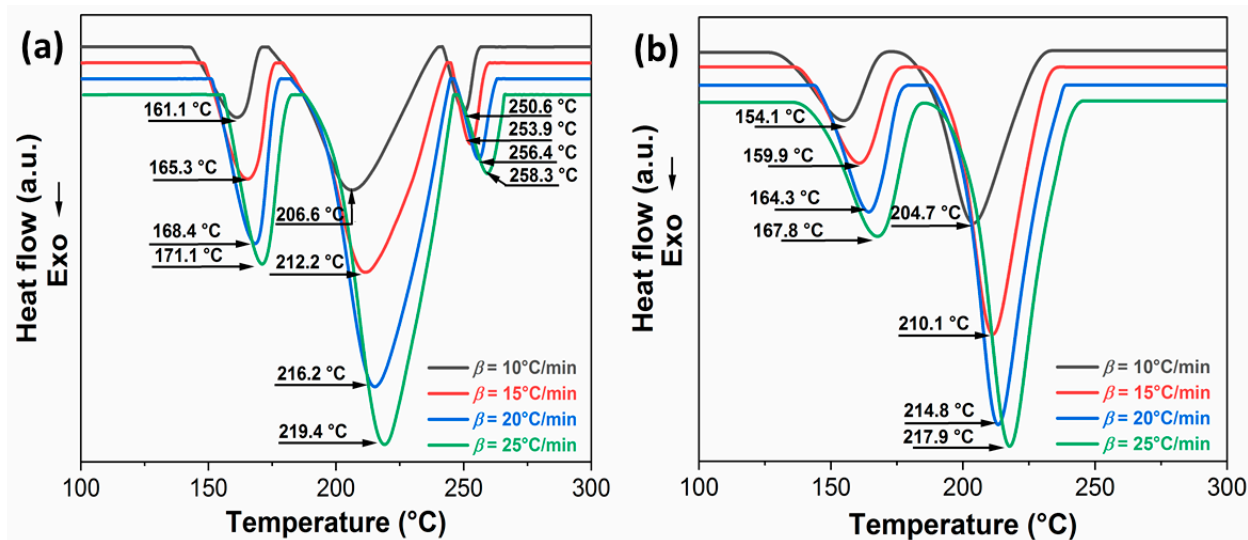


**Figure 4.** DSC curves of the (a) NC/HNTO/MgAl-CuO and (b) NNC/HNTO/MgAl-CuO composites at different heating rates.

**Table 1.** DSC parameters of the NC/HNTO/MgAl-CuO and NNC/HNTO/MgAl-CuO composites.

Sample	Heating Rate (°C·mn <sup>-1</sup> )	Decomposition Stage	$T_{onset}$ (°C)	$T_{peak}$ (°C)	$\Delta H$ (J·g <sup>-1</sup> )	$\Delta H_T$ (J·g <sup>-1</sup> )
NC/HNTO/MgAl-CuO	10 °C/min	1st decomposition stage	135.7	161.1	198.3	875.6
		2nd decomposition stage	189.4	206.6	589.7	
		3rd decomposition stage	239.1	250.6	87.6	
	15 °C/min	1st decomposition stage	138.6	165.3	187.4	793.6
		2nd decomposition stage	190.2	212.2	511.9	
		3rd decomposition stage	237.27	253.9	71.9	
	20 °C/min	1st decomposition stage	141.7	168.4	178.7	825.8
		2nd decomposition stage	192.4	216.2	608.3	
		3rd decomposition stage	240.5	256.4	41.8	
	25 °C/min	1st decomposition stage	145.9	171.1	152.5	753.4
		2nd decomposition stage	194.4	219.4	581.4	
		3rd decomposition stage	246.5	258.3	19.51	
NNC/HNTO/MgAl-CuO	10 °C/min	1st decomposition stage	134.7	154.1	212.5	1477.0
		2nd decomposition stage	187.2	204.7	1264.5	
	15 °C/min	1st decomposition stage	135.7	159.9	230.9	1520.0
		2nd decomposition stage	185.9	210.1	1289.1	
	20 °C/min	1st decomposition stage	144.3	164.3	244.8	1418.2
		2nd decomposition stage	187.6	214.8	1173.4	
	25 °C/min	1st decomposition stage	143.8	167.8	263.8	1423.4
		2nd decomposition stage	193.8	217.9	1159.6	

$\Delta H$ : Enthalpy of decomposition;  $T_{onset}$ : Onset temperature of decomposition;  $T_{peak}$ : Peak temperature of decomposition.

According to Figure 4, the NC/HNTO/MgAl-CuO composite undergoes three exothermic decomposition events; however, only two exothermic processes are observed for the NNC/HNTO/MgAl-CuO composite, similar to what is found by the TGA characteri-

zations. The first decomposition peak for both energetic composites is related to the thermolysis of nitrate ester binders, where the main produced species, identified using TG-FTIR, were found to be  $N_xO_y/CO_2$  [42], whereas the other exothermic events are attributed to the high and low decomposition stages of HNTO salt [19]. Additionally, it is obvious from Table 1 and Figure 4 that the maximum decomposition temperature of the first and second peaks of the NNC/HNTO/MgAl-CuO (e.g.,  $T_{peak1} = 154$  °C and  $T_{peak2} = 204$  °C at 10 °C/min) formulation is lower than that of NC/HNTO/MgAl-CuO (e.g.,  $T_{peak1} = 161$  °C and  $T_{peak2} = 206$  °C at 10 °C/min), which is even lower than that of the NC/HNTO (e.g.,  $T_{peak1} = 201$  °C and  $T_{peak2} = 225$  °C at 10 °C/min) and NNC/HNTO (e.g.,  $T_{peak1} = 195$  °C and  $T_{peak2} = 209$  °C at 10 °C/min) baselines [43], supporting the TGA/DTG results. Another interesting result is that the  $\Delta H_T$  of NNC/HNTO/MgAl-CuO (e.g.,  $1520 \text{ J}\cdot\text{g}^{-1}$  at 15 °C/min) is higher than that of NC/HNTO/MgAl-CuO (e.g.,  $793.6 \text{ J}\cdot\text{g}^{-1}$  at 15 °C/min), confirming once more the effectiveness of switching from NC to its nanostructured derivative as well as the role of MgAl-CuO nanothermite as a high-energy-density material that would increase heat production [44]. This claim was also confirmed by Tarchoun et al. [45] and Chen et al. [46], who confirmed that the substitution of nitrocellulose (NC) with its micro- or nanosized derivatives is a highly effective way to develop energetic nanocomposites with improved thermal reactivity and combustion performance. Additionally, Ningning Zhao and coworkers [41] demonstrated that the incorporation of Al/CuO nanothermites within energetic formulations shows unique catalytic activities in accelerating the thermolysis of nitrocellulose (NC) and combustion characteristics of the AP/HTPB propellant. It is worth noting that, according to the obtained findings, the thermolysis process of (NC and NNC) might principally control the thermal behavior of the obtained energetic formulations. Furthermore, it is crucial to note that the newly developed NC/HNTO/MgAl-CuO and NNC/HNTO/MgAl-CuO composites have a lower temperature of decomposition than certain reported nitrocellulose-based energetic formulations, such as (NC/Glycidyl Azid Polymer,  $T_{peak} = 193.28$  °C at  $\beta = 10$  °C/min); (NC/GAP/submicron-Hexa-Nitro-Stilbene,  $T_{peak} = 178$  °C at  $\beta = 10$  °C/min) [47]; and (Al/Fe<sub>2</sub>O<sub>3</sub>/NC,  $T_{1,exo} = 201.4$  °C at  $\beta = 10$  °C/min; Al/Fe<sub>2</sub>O<sub>3</sub>/RDX/NC,  $T_{1,exo} = 206.2$  °C at  $\beta = 10$  °C/min) [48].

#### 2.4. Determination of the Decomposition Kinetic Parameters

To investigate the thermo-kinetic mechanism of the exothermic decomposition stages of the developed energetic composites and accurately master their thermal reactivity, their key kinetic parameters ( $E_a$ ,  $\text{Log}(A)$ , and  $g(\alpha)$ ) were calculated on the basis of DSC data.

The isoconversional integral methods employed in this work to predict the kinetic triplet are VYA/CE, it-KAS, and TAS. Figures 5 and 6 show the variation in the Arrhenius parameters versus conversion for each thermolysis process that occurred in the elaborated energetic formulations. The average values of the Arrhenius parameters, with their related uncertainties and the mathematical reaction mechanism, are listed in Table 2.

**Table 2.** Thermo-kinetic parameters of the developed energetic formulations.

Sample	Kinetic Method	$E_a$ (kJ/mol)	$\text{Log}(A)$ (s <sup>-1</sup> )	$g(\alpha)$	
NC-HNTO-MgAlCuO 1st step	TAS	$130.93 \pm 15.22$	$13.93 \pm 3.24$	$A_{3/2} = [-\ln(1 - \alpha)]^{2/3}$	
	it-KAS	$130.90 \pm 15.22$	$13.72 \pm 3.19$	$R1, F0, P1 = \alpha$	
	VYA/CE	$\beta = 10$ °C/min	$130.73 \pm 15.19$	$13.64 \pm 3.17$	/
		$\beta = 15$ °C/min		$13.64 \pm 3.17$	/
		$\beta = 20$ °C/min		$13.70 \pm 3.19$	/
		$\beta = 25$ °C/min		$13.67 \pm 3.18$	/

Table 2. Cont.

Sample	Kinetic Method	$E_a$ (kJ/mol)	$\text{Log}(A)$ ( $\text{s}^{-1}$ )	$g(\alpha)$	
NC-HNTO-MgAlCuO 2nd step	TAS	$137.94 \pm 13.54$	$12.94 \pm 1.41$	$A_3 = [-\ln(1 - \alpha)]^{1/3}$	
	it-KAS	$137.89 \pm 13.55$	$12.96 \pm 1.41$	$A_{3/4} = [-\ln(1 - \alpha)]^{4/3}$	
	VYA/CE	$\beta = 10^\circ\text{C}/\text{min}$	$137.68 \pm 13.53$	$12.48 \pm 1.40$	/
		$\beta = 15^\circ\text{C}/\text{min}$		$12.47 \pm 1.40$	/
		$\beta = 20^\circ\text{C}/\text{min}$		$12.50 \pm 1.41$	/
$\beta = 25^\circ\text{C}/\text{min}$		$12.58 \pm 1.42$		/	
NC-HNTO-MgAlCuO 3rd step	TAS	$280.4 \pm 18.84$	$26.28 \pm 0.93$	$A_4 = [-\ln(1 - \alpha)]^{1/4}$	
	it-KAS	$280.36 \pm 18.84$	$25.98 \pm 0.92$	$G_7 = [1 - (1 - \alpha)^{1/2}]^{1/2}$	
	VYA/CE	$\beta = 10^\circ\text{C}/\text{min}$	$280.24 \pm 18.83$	$26.06 \pm 0.92$	/
		$\beta = 15^\circ\text{C}/\text{min}$		$26.04 \pm 0.92$	/
		$\beta = 20^\circ\text{C}/\text{min}$		$26.01 \pm 0.92$	/
$\beta = 25^\circ\text{C}/\text{min}$		$25.98 \pm 0.91$		/	
NNC-HNTO-MgAlCuO 1st step	TAS	$104.41 \pm 13.61$	$10.53 \pm 1.78$	$E_1 = \ln \alpha$	
	it-KAS	$104.35 \pm 13.60$	$10.59 \pm 1.79$	$R_1, F_0, P_1 = \alpha$	
	VYA/CE	$\beta = 10^\circ\text{C}/\text{min}$	$104.13 \pm 13.57$	$10.34 \pm 1.75$	/
		$\beta = 15^\circ\text{C}/\text{min}$		$10.39 \pm 1.76$	/
		$\beta = 20^\circ\text{C}/\text{min}$		$10.40 \pm 1.76$	/
$\beta = 25^\circ\text{C}/\text{min}$		$10.34 \pm 1.75$		/	
NNC-HNTO-MgAlCuO 2nd step	TAS	$131.51 \pm 18.21$	$12.15 \pm 2.11$	$E_1 = \ln \alpha$	
	it-KAS	$131.45 \pm 18.20$	$12.85 \pm 2.23$	$A_1 = -\ln(1 - \alpha)$	
	VYA/CE	$\beta = 10^\circ\text{C}/\text{min}$	$131.24 \pm 18.17$	$12.80 \pm 2.22$	/
		$\beta = 15^\circ\text{C}/\text{min}$		$12.83 \pm 2.23$	/
		$\beta = 20^\circ\text{C}/\text{min}$		$12.96 \pm 2.25$	/
$\beta = 25^\circ\text{C}/\text{min}$		$12.84 \pm 2.23$		/	

The main result is that the three utilized isoconversional integral methods (VYA/CE, it-KAS, and TAS) provide very accurate values of  $E_a$  and  $\text{Log}(A)$  for both the NC/HNTO/MgAl-CuO and NNC/HNTO/MgAl-CuO composites, with a relative standard error of less than 20%, demonstrating the excellent predictive power of the selected model-free methods and indicating the accuracy of the computed parameters [49,50]. Additional support for the high accuracy of the linear TAS and it-KAS models comes from the strong regression coefficient ( $R^2$ ), which ranges between 0.9980 and 0.9998. Another interesting finding is that, for each thermolysis stage, the three employed isoconversional methods provide a similar evolution trend of  $E_a$  and  $\text{Log}(A)$  versus conversion, confirming the kinetic compensation effect for the investigated composites [51].

According to Figures 5 and 6, there is an increase in  $E_a$  and  $\log(A)$  as a function of conversion in the first and second stages of decomposition for both energetic composites. Meanwhile, it is important to note that the mean  $E_a$  values obtained for the first thermolysis process, related to the thermolytic splitting of O-NO<sub>2</sub> groups of NNC/HNTO/MgAl-CuO composite (~104 kJ/mol), are lower than those of the NC/HNTO/MgAl-CuO composite (~139 kJ/mol), which are even lower than those of the NC/HNTO (~139 kJ/mol) and NNC/HNTO (~119 kJ/mol) baselines, as well as NC (~172 kJ/mol) and NNC (~156 kJ/mol) binders [43,52]. These findings indicate that MgAl-CuO nanothermite is a key factor in accelerating the thermolysis of nitrated cellulose chains through the physical adsorption of the nitrous oxides in the active sites of the nanothermite solid surface, which will inhibit

their diffusion to the outer atmosphere, therefore, keeping the  $\text{NO}_2$  molecules stagnant within the NC-based formulation and, hence, increasing the autocatalytic thermal decomposition of the NC/HNTO and NNC/HNTO composites [41]. Additionally, the large specific surface area of MgAl-CuO nanothermite can improve the autocatalytic process of NC via the adsorption of  $\text{NO}_2$  molecules produced during its intrinsic decomposition [27,53]. A similar effect was observed in the research work of Benhammada et al. [38]. The authors reported that iron oxide nanoparticles decorated on carbon mesospheres provide a strong catalytic effect after the initial decomposition of NC, decreasing the thermolysis activation energy. Concerning the second decomposition step, assigned to the simultaneous decomposition of nitro, hydrazine, and carbonyl functions accompanied by azole ring cleavage, both the NC/HNTO/MgAl-CuO and NNC/HNTO/MgAl-CuO formulations display a similar growing trend of Arrhenius parameters. This indicates that the second decomposition process is much easier at the beginning of conversion, which is caused by the autocatalytic species released during the intrinsic decomposition of nitrate esters. The decomposition significantly decreased the initiation energy of raw HNTO salt, which generally ranged between 180 and 200 kJ/mol [19,22]. Furthermore, Figures 5 and 6 depict a decay profile of Arrhenius factors as a function of conversion for the final stage of the NC/HNTO/MgAlCuO composite's decomposition, which is related to the post-decomposition of residual HNTO. Additionally, it is important to note that the kinetic parameters during the two parts of decomposition of NNC/HNTO/MgAl-CuO are found to be lower than the NC/HNTO/MgAl-CuO, thereby correlating with the thermal results.

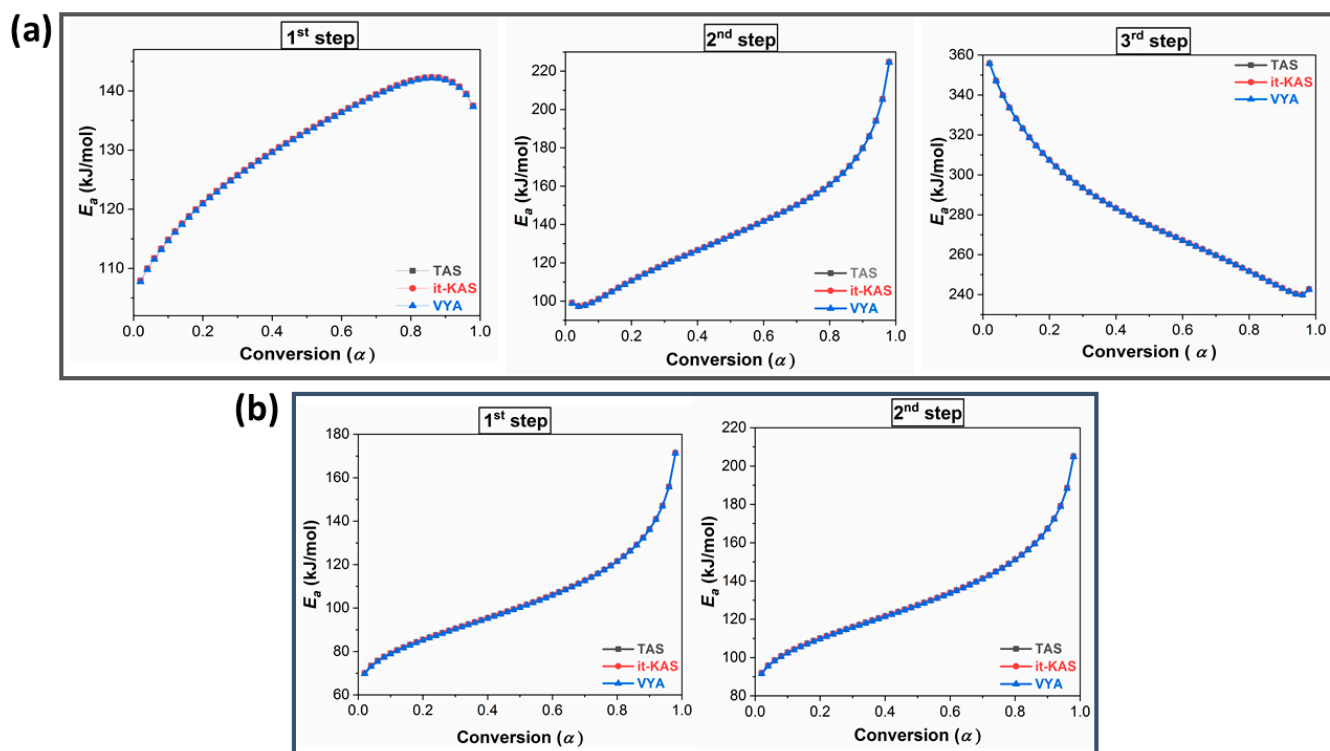


**Figure 5.** Evolution of the activation energy as a function of conversion for each decomposition step of (a) NC/HNTO/MgAlCuO; (b) NNC/HNTO/MgAlCuO.

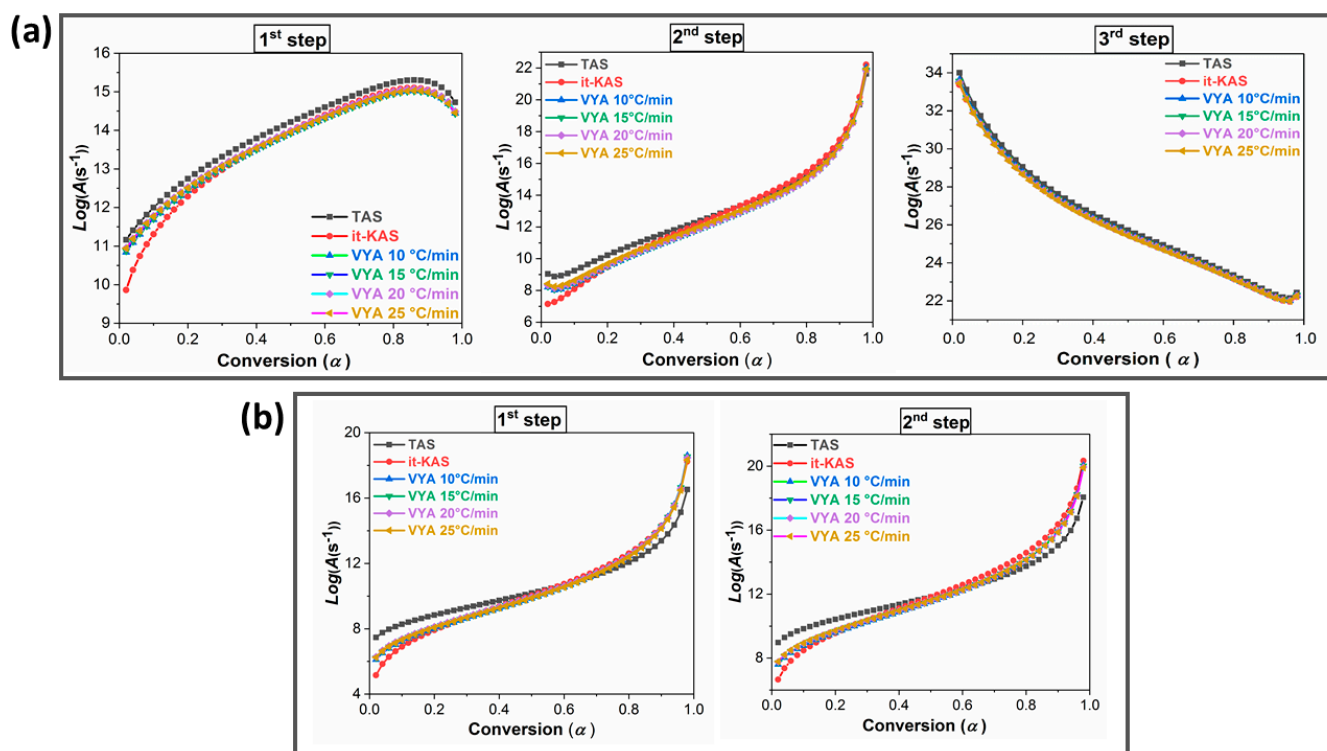


**Figure 6.** Evolution of the frequency factor as a function of conversion for each decomposition step of (a) NC/HNTO/MgAlCuO; (b) NNC/HNTO/MgAlCuO.

The evaluation of the most probable reaction models ( $g(\alpha)$ ) of these newly developed energetic formulations is another important factor to take into account when examining the thermo-kinetic behavior. Figure 7 shows the evolution of the models as a function of conversion, while their mathematical formulas are listed in Table 2. It is worth noting that the Vyazovkin non-linear approach does not enable the acquisition of the reaction model, but it provides numerical values of  $g(\alpha)$  when combined with the compensation effect. Based on the 41 theoretical models that we recently presented [54], the systems under investigation decompose following different models. According to the TAS method, the decomposition processes of the NC/HNTO/MgAl-CuO composite are controlled by random Avrami-Erofeev nucleation ( $A_{19}$ ,  $A_{23}$ , and  $A_{24}$ , respectively) during the three decomposition stages, while the decomposition processes of the NNC/HNTO/MgAl-CuO composite are governed by nucleation (exponential law, E1) during the two decomposition steps. However, the it-KAS method indicates that the first decomposition process of both composites follows a contracting disk ( $R_1$ ,  $F_0$ ,  $P_1$ ), whereas the second decomposition process of NC/HNTO/MgAl-CuO and NNC/HNTO/MgAl-CuO composites is controlled by random nucleation Avrami-Erofeev ( $A_{3/4}$ ) and Random nucleation/first-order Mampel ( $A_1$ ), respectively. The last decomposition step for the NC/HNTO/MgAl-CuO composite is governed by unjustified mechanisms ( $G_7$ ). It is also crucial to note that the thermo-kinetic parameters of the newly developed energetic formulations were in excellent agreement with the kinetic findings of the same type of NC-based formulations disclosed in the open literature [55]. As a result, the current thermo-kinetic findings obtained in this study offer excellent insights into the importance of developing new nano-energetic formulations based on nitrated cellulosic polymers, HNTO, and nanothermite MgAl-CuO for potential use in solid propellants and explosive formulations.

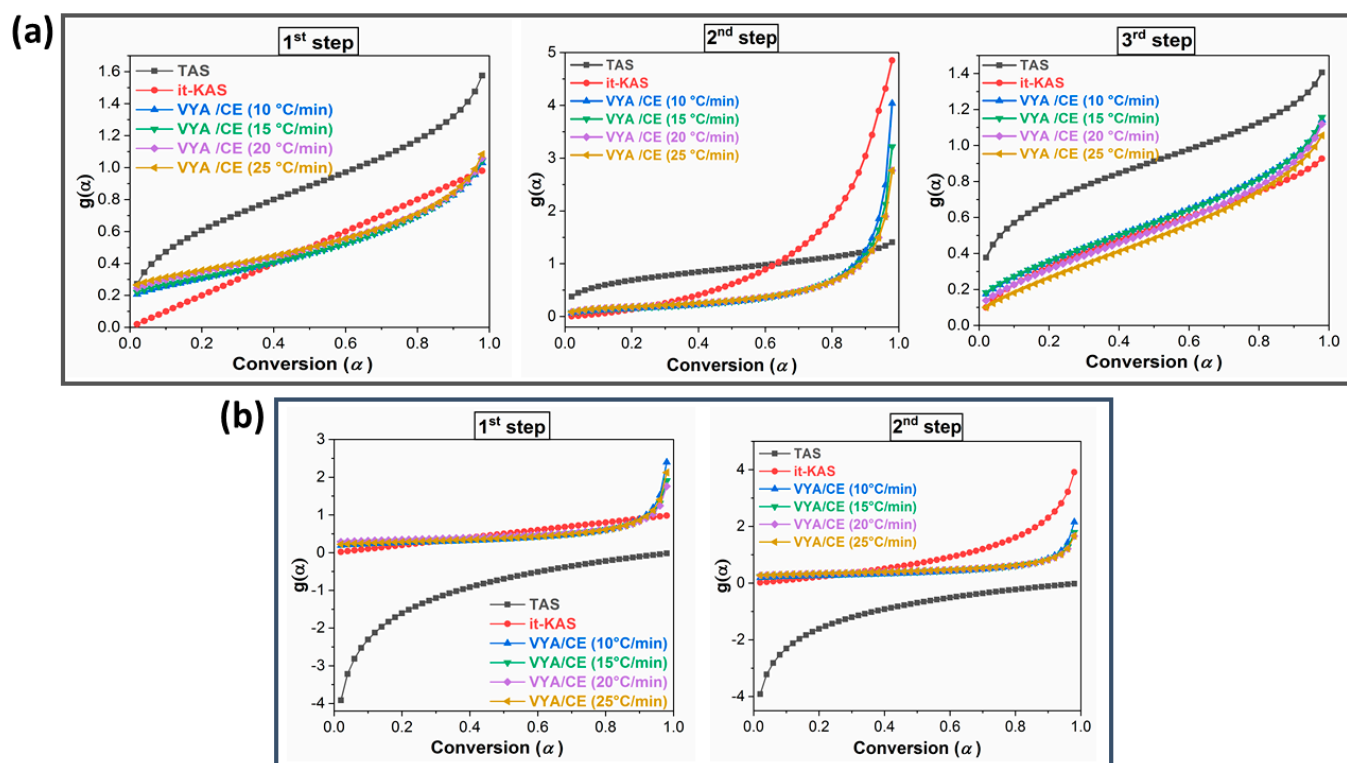


**Figure 7.** Variation in integral reaction model as a function of conversion for each decomposition step of (a) NC/HNTO/MgAlCuO; (b) NNC/HNTO/MgAlCuO.

### 3. Experimental Section

#### 3.1. Materials

Nitrated cellulose (NC) and nanostructured nitrocellulose (NNC) with nitration degrees of 12.61% and 13.08%, correspondingly, were fabricated in our EMLab using the nitration method outlined in our latest papers [8,52]. Hydrazinium nitro-triazolone (HNTO, 99.5%) had already been synthesized using a mixture of hydrazine hydrate and 3-nitro-2,4-dihydro-3H-1,2,4-triazole-5-one (NTO) according to the process described by Hanafi and coworkers [56]. MgAl-CuO ternary nanothermite, based on fuel-rich nanopowders (Mg, Al, CuO), was prepared using the arrested milling process, which allows one to obtain uniform nanoscale MgAl-CuO nanothermite. The prepared catalyst was thoroughly characterized as mentioned in our recent study [53].

#### 3.2. Preparation of the Energetic Formulations

The NC/HNTO/MgAl-CuO and NNC/HNTO/MgAl-CuO formulations were fabricated by mixing 38 wt.% of nitrated cellulosic polymer (NC or NNC), 57 wt.% of HNTO, and 5 wt.% of MgAl-CuO. It should be mentioned that the mass fractions of the employed compounds are determined based on the results given in our latest investigations [43,53].

As depicted in Figure 1, dried NC (or NNC) was initially dissolved in a sufficient amount of acetone under stirring at 20 °C for 30 min. Next, the dried HNTO was slowly incorporated into the mixture under continuous stirring. A few mL of acetone should be added throughout the mixing process to prevent the mixture's viscosity from decreasing due to the high volatility of acetone. After that, the dried MgAl-CuO nanopowder was dissolved in 40 mL of acetone and sonicated for 15 min to produce a black emulsion. The obtained nanothermite solution was added to the NC (or NNC)/HNTO mixture under stirring for 1 h. Lastly, the resulting mixtures were dried, forming thin films of NC/HNTO/MgAl-CuO and NNC/HNTO/MgAl-CuO. The preparation pathway of the developed energetic formulations is presented in Figure 8.

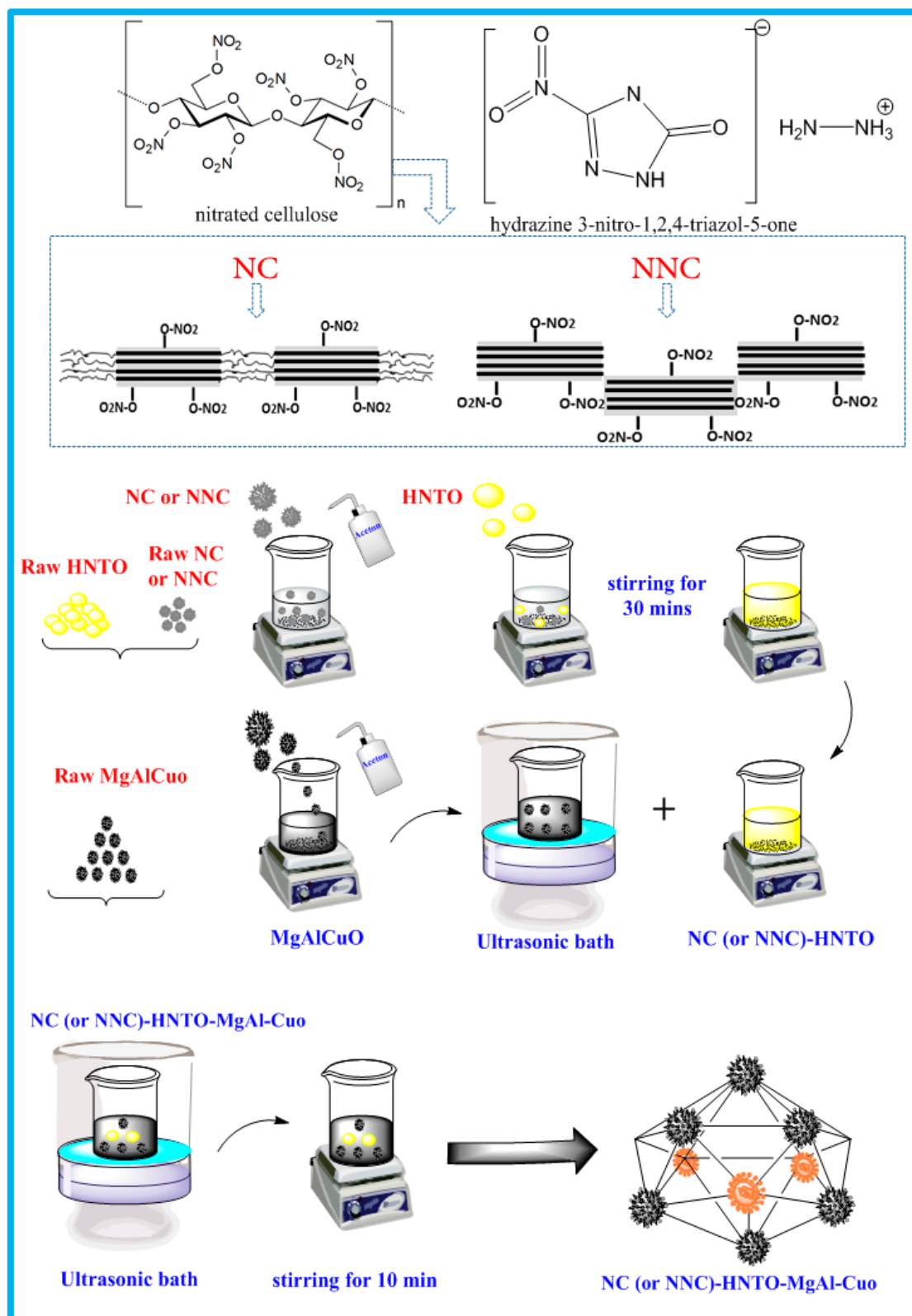


**Figure 8.** Preparation process of NC (or NNC)/HNTO/MgAl-CuO composites.

### 3.3. Characterization Techniques

Fourier-transform infrared spectroscopy (FTIR, Perkin-Elmer 1600, USA) was employed to characterize the chemical structure of the developed energetic composites. The spectra, within a range of  $4000\text{--}400\text{ cm}^{-1}$ , were obtained in Attenuated Total Reflection

mode with a resolution of  $4 \text{ cm}^{-1}$ . The morphology of the prepared energetic formulations and their raw compounds was characterized by scanning electron microscopy (SEM, FEI Quanta 600, USA). Thermogravimetric analysis (TGA) and differential scanning calorimetry (DSC) techniques were utilized to elucidate the thermal decomposition behavior of the elaborated energetic composites. TGA (Perkin–Elmer 4000 analyzer, USA) and DSC (Perkin–Elmer 8000 analyzer, USA) experiments, for about 0.5–1.5 mg samples, were recorded under 30 mL/min nitrogen atmosphere from 50 to 350 °C at a heating rate of 10 °C/min for TGA, while at distinct heating rates (10, 15, 20, and 25 °C/min) for DSC.

### 3.4. Kinetic Decomposition Parameters

In order to elucidate the thermo-kinetic mechanisms of the designed energetic formulations, their thermo-kinetic behaviors were investigated based on DSC experiments and using kinetic approaches. In this study, we respected the recommendation of the International Confederation for Thermal Analysis and Calorimetry (ICTAC) (Equation (1)) [57], where  $k(T)$  is the rate constant at the temperature  $T$ . The temperature dependence of  $k(T)$  is commonly expressed by the Arrhenius equation; therefore,  $A$ ,  $E_a$ , and  $R$  are the Arrhenius pre-exponential factor, apparent activation energy, and gas constant, respectively. Herein,  $f(\alpha)$  is the differential form of the mathematical function that describes the reaction model that represents the reaction mechanism and for the integral methods is noted as  $g(\alpha)$  given by Equation (2) [58,59].

$$\frac{d\alpha}{dT} = k(T)f(\alpha) = Ae^{(\frac{-E_a}{RT})}f(\alpha) \quad (1)$$

$$g(\alpha) = \int_0^{\alpha} \frac{d\alpha}{f(\alpha)} \quad (2)$$

The conversion ( $\alpha$ ) is determined from DSC thermograms as a ratio of the current heat change  $\Delta H$  to the total reaction heat  $\Delta H_{total}$ .

$$\alpha = \frac{\int_{t_0}^t (dH/dt)dt}{\int_{t_0}^{t_f} (dH/dt)dt} = \frac{\Delta H}{\Delta H_{total}} \quad (3)$$

In this study, the kinetic parameters ( $E_a$ ,  $\text{Log}(A)$ ,  $g(\alpha)$ ) were calculated using two linear integral methods, namely Trache-Abdelaziz-Siwani (TAS) [54] and the iterative Kissinger-Akahira-Sunose (it-KAS) [60], as well as one non-linear Vyazovkin approach (VYA) coupled with the compensation effect approach (CE) [58]. The calculations were carried out using a local code compiled in MATLAB software (2007b, USA) [61,62].

## 4. Conclusions

In this study, promising energetic formulations based on HNTO explosive, nitrated cellulosic polymers (NC and NNC), and nanothermite were successfully elaborated through a casting method. Structural characterizations (FTIR and SEM) of the obtained energetic formulations demonstrated their homogeneity, with significant dispersion of the nanothermite inside the nitrated cellulosic chains and HNTO matrices. The nanostructured NNC/HNTO/MgAl-CuO composite possessed lower decomposition temperatures and lower activation energies than the NC/HNTO/MgAl-CuO composite. Additionally, a higher heat release and a considerable decrease in the activation energy were observed for both composites, confirming the improved thermal reactivity of the nanostructured nitrated cellulose and the highest catalytic performance of the nanothermite. Additionally, the calculated isoconversional kinetic methods demonstrated that the produced energetic composites follow a variety of decomposition mechanisms, ranging from nucleation to an Avrami-Erofeev random nucleation mechanism. Based on these findings, a promising high-energy nanocomposite, based on nanostructured nitrocellulose, hydrazinium nitro-

triazolone, and copper oxide-magnesium-aluminum nanothermite, can be viewed as an innovative formulation for the development of advanced composite explosives and solid rocket propellants.

**Author Contributions:** M.D.: Conceptualization, Methodology, Resources, Investigation, data treatment, Writing-Original Draft. A.F.T.: Supervision, Conceptualization, Review & Editing. D.T.: Supervision, Conceptualization, Review & Editing. A.A., S.B., A.H., H.B. and N.M.: Review & Editing the manuscript draft. All authors have read and agreed to the published version of the manuscript.

**Funding:** The authors do not have any funding or financial support to declare.

**Data Availability Statement:** Available data are presented in the manuscript.

**Conflicts of Interest:** The authors declare that they have no conflict of interest.

## References

1. Trache, D.; DeLuca, L.T. Nanoenergetic Materials: Preparation, Properties, and Applications. *Nanomaterials* **2020**, *10*, 2347. [[CrossRef](#)] [[PubMed](#)]
2. Kabra, S.; Gharde, S.; Gore, P.M.; Jain, S.; Khire, V.H.; Kandasubramanian, B. Recent trends in nanothermites: Fabrication, characteristics and applications. *Nano Express* **2020**, *1*, 032001. [[CrossRef](#)]
3. Trache, D.; Tarchoun, A.F. Differentiation of stabilized nitrocellulose during artificial aging: Spectroscopy methods coupled with principal component analysis. *J. Chemom.* **2019**, *33*, e3163. [[CrossRef](#)]
4. Gismatulina, Y.A.; Budaeva, V.V.; Sakovich, G.V. Nitrocellulose synthesis from miscanthus cellulose. *Propellants Explos. Pyrotech.* **2018**, *43*, 96–100. [[CrossRef](#)]
5. Okada, K.; Saito, Y.; Akiyoshi, M.; Endo, T.; Matsunaga, T. Preparation and characterization of nitrocellulose nanofiber. *Propellants Explos. Pyrotech.* **2021**, *46*, 962–968. [[CrossRef](#)]
6. Tarchoun, A.F.; Trache, D.; Derradji, M.; Bessa, W.; Belgacemi, R. Cellulose nanoparticles: Extractions. In *Cellulose Nanoparticles: Chemistry and Fundamentals*; Royal Society of Chemistry: London, UK, 2021; pp. 113–148.
7. Rani, A.; Reddy, R.; Sharma, U.; Mukherjee, P.; Mishra, P.; Kuila, A.; Sim, L.C.; Saravanan, P. A review on the progress of nanostructure materials for energy harnessing and environmental remediation. *J. Nanostructure Chem.* **2018**, *8*, 255–291. [[CrossRef](#)]
8. Tarchoun, A.F.; Sayah, Z.B.D.; Trache, D.; Klapötke, T.M.; Belmerabt, M.; Abdelaziz, A.; Bekhouche, S. Towards investigating the characteristics and thermal kinetic behavior of emergent nanostructured nitrocellulose prepared using various sulfonitric media. *J. Nanostructure Chem.* **2022**, *12*, 963–977. [[CrossRef](#)]
9. Pourmortazavi, S.M.; Kohsari, I.; Zandavar, H.; Foroutan Koudehi, M.; Mirsadeghi, S. Electrospinning and thermal characterization of nitrocellulose nanofibers containing a composite of diaminofurazan, aluminum nano-powder and iron oxide nanoparticles. *Cellulose* **2019**, *26*, 4405–4415. [[CrossRef](#)]
10. Rozumov, E. Recent Advances in Gun Propellant Development: From Molecules to Materials. *Energetic Mater.* **2017**, *25*, 23–65.
11. Ye, B.; An, C.; Wang, J.; Li, H.; Ji, W.; Gao, K. Preparation and characterization of RDX-based composite with glycidyl azide polymers and nitrocellulose. *J. Propuls. Power* **2016**, *32*, 1036–1040. [[CrossRef](#)]
12. Shi, X.; Wang, J.; Li, X.; An, C. Preparation and properties of HMX/nitrocellulose nanocomposites. *J. Propuls. Power* **2015**, *31*, 757–761. [[CrossRef](#)]
13. Trache, D.; Klapötke, T.M.; Maiz, L.; Abd-Elghany, M.; DeLuca, L.T. Recent advances in new oxidizers for solid rocket propulsion. *Green Chem.* **2017**, *19*, 4711–4736. [[CrossRef](#)]
14. Liang, X.; Jiang, H.; Pan, X.; Hua, M.; Jiang, J. Analysis and characterization of nitrocellulose as binder optimized by 1-butyl-3-methylimidazolium bis (trifluoromethylsulfonyl) imide. *J. Therm. Anal. Calorim.* **2021**, *143*, 113–126. [[CrossRef](#)]
15. Lysien, K.; Stolarczyk, A.; Jarosz, T. Solid Propellant Formulations: A Review of Recent Progress and Utilized Components. *Materials* **2021**, *14*, 6657. [[CrossRef](#)] [[PubMed](#)]
16. Dai, J.; Wang, C.; Wang, Y.; Xu, W.; Xu, J.; Shen, Y.; Zhang, W.; Ye, Y.; Shen, R. From nanoparticles to on-chip 3D nanothermite: Electro spray deposition of reactive Al/CuO@NC onto semiconductor bridge and its application for rapid ignition. *Nanotechnology* **2020**, *31*, 195712. [[CrossRef](#)]
17. Luo, Y.; Zheng, W.; Wang, X.; Shen, F. Nitrification Progress of Nitrogen-Rich Heterocyclic Energetic Compounds: A Review. *Molecules* **2022**, *27*, 1465. [[CrossRef](#)]
18. Srinivas, D.; Ghule, V.D.; Muralidharan, K.; Jenkins, H.D.B. Tetraanionic Nitrogen-Rich Tetrazole-Based Energetic Salts. *Chem.-Asian J.* **2013**, *8*, 1023–1028. [[CrossRef](#)]
19. Yi, J.-H.; Zhao, F.-Q.; Gao, H.-X.; Xu, S.-Y.; Wang, M.-C. Preparation, characterization, non-isothermal reaction kinetics, thermodynamic properties, and safety performances of high nitrogen compound: Hydrazine 3-nitro-1,2,4-triazol-5-one complex. *J. Hazard. Mater.* **2008**, *153*, 261–268. [[CrossRef](#)]
20. Abdelaziz, A.; Tarchoun, A.F.; Boukeciat, H.; Trache, D. Insight into the Thermodynamic Properties of Promising Energetic HNTO·AN Co-Crystal: Heat Capacity, Combustion Energy, and Formation Enthalpy. *Energies* **2022**, *15*, 6722. [[CrossRef](#)]

21. Zhang, M.; Li, C.; Gao, H.; Fu, W.; Li, Y.; Tang, L.; Zhou, Z. Promising hydrazinium 3-Nitro-1, 2, 4-triazol-5-one and its analogs. *J. Mater. Sci.* **2016**, *51*, 10849–10862. [[CrossRef](#)]
22. He, W.; Liu, P.J.; He, G.Q.; Gozin, M.; Yan, Q.L. Highly reactive metastable intermixed composites (MICs): Preparation and characterization. *Adv. Mater.* **2018**, *30*, 1706293. [[CrossRef](#)] [[PubMed](#)]
23. Deng, J.; Li, G.; Shen, L.; Luo, Y. Application of Al/B/Fe<sub>2</sub>O<sub>3</sub> nano thermite in composite solid propellant. *Bull. Chem. React. Eng. Catal.* **2016**, *11*, 109–114. [[CrossRef](#)]
24. Zhu, Y.; Zhou, X.; Xu, J.; Ma, X.; Ye, Y.; Yang, G.; Zhang, K. In situ preparation of explosive embedded CuO/Al/CL20 nanoenergetic composite with enhanced reactivity. *Chem. Eng. J.* **2018**, *354*, 885–895. [[CrossRef](#)]
25. Baer, M. Modeling heterogeneous energetic materials at the mesoscale. *Thermochim. Acta* **2002**, *384*, 351–367. [[CrossRef](#)]
26. Chowdhury, S.; Sullivan, K.; Piekielek, N.; Zhou, L.; Zachariah, M.R. Diffusive vs explosive reaction at the nanoscale. *J. Phys. Chem. C* **2010**, *114*, 9191–9195. [[CrossRef](#)]
27. Yao, E.; Zhao, N.; Qin, Z.; Ma, H.; Li, H.; Xu, S.; An, T.; Yi, J.; Zhao, F. Thermal decomposition behavior and thermal safety of nitrocellulose with different shape CuO and Al/CuO nanothermites. *Nanomaterials* **2020**, *10*, 725. [[CrossRef](#)]
28. Dolgachev, V.; Khanefat, A.; Mitrofanov, A. Ignition of organic explosive materials by a copper oxide film absorbing a laser pulse. *Propellants Explos. Pyrotech.* **2018**, *43*, 992–998. [[CrossRef](#)]
29. Trache, D.; Khimeche, K.; Mezroua, A.; Benziane, M. Physicochemical properties of microcrystalline nitrocellulose from Alfa grass fibres and its thermal stability. *J. Therm. Anal. Calorim.* **2016**, *124*, 1485–1496. [[CrossRef](#)]
30. Dave, P.N.; Thakkar, R.; Sirach, R.; Chaturvedi, S. Effect of copper ferrite (CuFe<sub>2</sub>O<sub>4</sub>) in the thermal decomposition of modified nitrotriazolone. *Mater. Adv.* **2022**, *3*, 5019–5026. [[CrossRef](#)]
31. Tarchoun, A.F.; Trache, D.; Klapötke, T.M.; Chelouche, S.; Derradji, M.; Bessa, W.; Mezroua, A. A promising energetic polymer from Posidonia oceanica brown algae: Synthesis, characterization, and kinetic modeling. *Macromol. Chem. Phys.* **2019**, *220*, 1900358. [[CrossRef](#)]
32. Benhammada, A.; Trache, D. Green synthesis of CuO nanoparticles using Malva sylvestris leaf extract with different copper precursors and their effect on nitrocellulose thermal behavior. *J. Therm. Anal. Calorim.* **2022**, *147*, 1–16. [[CrossRef](#)]
33. Wang, H.; Jian, G.; Yan, S.; DeLisio, J.B.; Huang, C.; Zachariah, M.R. Electrospray formation of gelled nano-aluminum microspheres with superior reactivity. *ACS Appl. Mater. Interfaces* **2013**, *5*, 6797–6801. [[CrossRef](#)] [[PubMed](#)]
34. Wu, Y.; Yi, Z.; Luo, Y.; Ge, Z.; Du, F.; Chen, S.; Sun, J. Fabrication and properties of glycidyl azide polymer-modified nitrocellulose spherical powders. *J. Therm. Anal. Calorim.* **2017**, *129*, 1555–1562. [[CrossRef](#)]
35. Yi, J.-H.; Zhao, F.-Q.; Ren, Y.-H.; Xu, S.-Y.; Ma, H.-X.; Hu, R.-Z. Thermal decomposition mechanism and quantum chemical investigation of hydrazine 3-nitro-1,2,4-triazol-5-one (HNTO). *J. Therm. Anal. Calorim.* **2010**, *100*, 623–627. [[CrossRef](#)]
36. Chen, L.; He, W.; Liu, J. Safe fabrication, thermal decomposition kinetics, and mechanism of nanoenergetic composite NBC/CL-20. *ACS Omega* **2020**, *5*, 31407–31416. [[CrossRef](#)] [[PubMed](#)]
37. Mezroua, A.; Hamada, R.A.; Brahmine, K.S.; Abdelaziz, A.; Tarchoun, A.F.; Boukeciat, H.; Bekhouche, S.; Bessa, W.; Benhammada, A.; Trache, D. Unraveling the role of ammonium perchlorate on the thermal decomposition behavior and kinetics of NC/DEGDN energetic composite. *Thermochim. Acta* **2022**, *716*, 179305. [[CrossRef](#)]
38. Benhammada, A.; Trache, D.; Kesraoui, M.; Chelouche, S. Hydrothermal synthesis of hematite nanoparticles decorated on carbon mesospheres and their synergetic action on the thermal decomposition of nitrocellulose. *Nanomaterials* **2020**, *10*, 968. [[CrossRef](#)] [[PubMed](#)]
39. Tarchoun, A.F.; Trache, D.; Klapötke, T.M.; Slimani, K.; Belouettar, B.e.; Abdelaziz, A.; Bekhouche, S.; Bessa, W. Valorization of esparto grass cellulosic derivatives for the development of promising energetic azidodeoxy biopolymers: Synthesis, characterization and isoconversional thermal kinetic analysis. *Propellants Explos. Pyrotech.* **2022**, *47*, e202100293. [[CrossRef](#)]
40. Dobrynin, O.S.; Zharkov, M.N.; Kuchurov, I.V.; Fomenkov, I.V.; Zlotin, S.G.; Monogarov, K.A.; Meerov, D.B.; Pivkina, A.N.; Muravyev, N.V. Supercritical antisolvent processing of nitrocellulose: Downscaling to nanosize, reducing friction sensitivity and introducing burning rate catalyst. *Nanomaterials* **2019**, *9*, 1386. [[CrossRef](#)] [[PubMed](#)]
41. Zhao, N.; Ma, H.; Yao, E.; Yu, Z.; An, T.; Zhao, F.; Yu, X. Influence of tailored CuO and Al/CuO nanothermites on the thermocatalytic degradation of nitrocellulose and combustion performance of AP/HTPB composite propellant. *Cellulose* **2021**, *28*, 8671–8691. [[CrossRef](#)]
42. Benhammada, A.; Trache, D. Thermal decomposition of energetic materials using TG-FTIR and TG-MS: A state-of-the-art review. *Appl. Spectrosc. Rev.* **2020**, *55*, 724–777. [[CrossRef](#)]
43. Tarchoun, A.F.; Trache, D.; Abdelaziz, A.; Harrat, A.; Boukecha, W.O.; Hamouche, M.A.; Boukeciat, H.; Dourari, M. Elaboration, Characterization and Thermal Decomposition Kinetics of New Nanoenergetic Composite Based on Hydrazine 3-Nitro-1,2,4-triazol-5-one and Nanostructured Cellulose Nitrate. *Molecules* **2022**, *27*, 6945. [[CrossRef](#)] [[PubMed](#)]
44. Elbasuney, S.; Yehia, M.; Hamed, A.; Mokhtar, M.; Gobara, M.; Saleh, A.; Elsaka, E.; El-Sayyad, G.S. Synergistic catalytic effect of thermite nanoparticles on HMX thermal decomposition. *J. Inorg. Organomet. Polym. Mater.* **2021**, *31*, 2293–2305. [[CrossRef](#)]
45. Tarchoun, A.F.; Trache, D.; Klapötke, T.M.; Abdelaziz, A.; Bekhouche, S.; Boukeciat, H.; Sahnoun, N. Making progress towards promising energetic cellulosic microcrystals developed from alternative lignocellulosic biomasses. *J. Energetic Mater.* **2022**, 1–26. [[CrossRef](#)]
46. Chen, L.; Cao, X.; Gao, J.; He, W.; Liu, J.; Wang, Y.; Zhou, X.; Shen, J.; Wang, B.; He, Y. Nitrated bacterial cellulose-based energetic nanocomposites as propellants and explosives for military applications. *ACS Appl. Nano Mater.* **2021**, *4*, 1906–1915. [[CrossRef](#)]

47. Wang, Y.; Luo, T.; Song, X.; Li, F. Electrospinning Preparation of NC/GAP/Submicron-HNS Energetic Composite Fiber and its Properties. *ACS Omega* **2019**, *4*, 14261–14271. [[CrossRef](#)]
48. Yang, H.; Liu, Y.; Huang, H.; Zhao, Y.; Song, K.; Wang, H.; Xie, W.; Cheng, Y.; Fan, X. Preparation and characterization of the Al/Fe<sub>2</sub>O<sub>3</sub>/RDX/NC nanocomposites by electrospray. *J. Therm. Anal. Calorim.* **2019**, *137*, 1615–1620. [[CrossRef](#)]
49. Vyazovkin, S.; Burnham, A.K.; Favregeon, L.; Koga, N.; Moukhina, E.; Pérez-Maqueda, L.A.; Sbirrazzuoli, N. ICTAC Kinetics Committee recommendations for analysis of multi-step kinetics. *Thermochim. Acta* **2020**, *689*, 178597. [[CrossRef](#)]
50. Granado, L.; Sbirrazzuoli, N. Isoconversional computations for nonisothermal kinetic predictions. *Thermochim. Acta* **2021**, *697*, 178859. [[CrossRef](#)]
51. Sbirrazzuoli, N. Determination of pre-exponential factors and of the mathematical functions  $f(\alpha)$  or  $G(\alpha)$  that describe the reaction mechanism in a model-free way. *Thermochim. Acta* **2013**, *564*, 59–69. [[CrossRef](#)]
52. Tarchoun, A.F.; Trache, D.; Klapötke, T.M.; Selmani, A.; Saada, M.; Chelouche, S.; Mezroua, A.; Abdelaziz, A. New insensitive high-energy dense biopolymers from giant reed cellulosic fibers: Their synthesis, characterization, and non-isothermal decomposition kinetics. *New J. Chem.* **2021**, *45*, 5099–5113. [[CrossRef](#)]
53. Bekhouche, S.; Trache, D.; Abdelaziz, A.; Tarchoun, A.F.; Chelouche, S.; Boudjellal, A.; Mezroua, A. Preparation and characterization of MgAl-CuO ternary nanothermite system by arrested reactive milling and its effect on the thermocatalytic decomposition of cellulose nitrate. *Chem. Eng. J.* **2022**, *453*, 139845. [[CrossRef](#)]
54. Trache, D.; Abdelaziz, A.; Siouani, B. A simple and linear isoconversional method to determine the pre-exponential factors and the mathematical reaction mechanism functions. *J. Therm. Anal. Calorim.* **2017**, *128*, 335–348. [[CrossRef](#)]
55. Chen, L.; Liu, S.; Cao, X.; Gao, J.; Wang, Y.; Qin, Y.; Zhang, Y.; Zhang, J.; Jin, G.; Wang, M. Fabrication of nitrocellulose-based nanoenergetic composites, study on its structure, thermal decomposition kinetics, mechanism, and sensitivity. *Nano Sel.* **2021**, *2*, 2225–2236. [[CrossRef](#)]
56. Hanafi, S.; Trache, D.; Meziani, R.; Boukciat, H.; Mezroua, A.; Tarchoun, A.F.; Derradji, M. Synthesis, characterization and thermal decomposition behavior of a novel HNTO/AN co-crystal as a promising rocket propellant oxidizer. *Chem. Eng. J.* **2021**, *417*, 128010. [[CrossRef](#)]
57. Koga, N.; Vyazovkin, S.; Burnham, A.K.; Favregeon, L.; Muravyev, N.V.; Perez-Maqueda, L.A.; Saggese, C.; Sánchez-Jiménez, P.E. ICTAC Kinetics Committee recommendations for analysis of thermal decomposition kinetics. *Thermochim. Acta* **2022**, *719*, 179384. [[CrossRef](#)]
58. Sbirrazzuoli, N. Determination of pre-exponential factor and reaction mechanism in a model-free way. *Thermochim. Acta* **2020**, *691*, 178707. [[CrossRef](#)]
59. Vyazovkin, S. Determining preexponential factor in model-free kinetic methods: How and why? *Molecules* **2021**, *26*, 3077. [[CrossRef](#)]
60. Trache, D.; Maggi, F.; Palmucci, I.; DeLuca, L.T. Thermal behavior and decomposition kinetics of composite solid propellants in the presence of amide burning rate suppressants. *J. Therm. Anal. Calorim.* **2018**, *132*, 1601–1615. [[CrossRef](#)]
61. Achour, S.; Hamada, B.; Baroudi, S.; Abdelaziz, A.; Rezagui, I.; Trache, D. Spectroscopic characterization and thermal decomposition kinetics of 1, 3-dibutyl-imidazolium bromide synthesized through a solvent-free and one-pot method. *J. Mol. Liq.* **2021**, *339*, 117266. [[CrossRef](#)]
62. Benhammada, A.; Trache, D.; Kesraoui, M.; Tarchoun, A.F.; Chelouche, S.; Mezroua, A. Synthesis and characterization of  $\alpha$ -Fe<sub>2</sub>O<sub>3</sub> nanoparticles from different precursors and their catalytic effect on the thermal decomposition of nitrocellulose. *Thermochim. Acta* **2020**, *686*, 178570. [[CrossRef](#)]